OPEN ACCESS

NUMERICAL SIMULATION OF THE ELECTROLYTE CONCENTRATION AND FLOW RATE IMPACT ON THE HYDROGEN EVOLUTION IN AN ALKALINE WATER ELECTROLYSIS SYSTEM

Mena Y. Mikhail[1], Ehab Ali[1], Radwan M. El-Zoheiry[2], Mohamed M. Mousa[1, 3]
[1]Basic Engineering Sciences Department, Benha Faculty of Engineering, Benha University, Egypt
[2]Mechanical Engineering Department, Benha Faculty of Engineering, Benha University, Egypt
[3]Faculty of Engineering Technology, Elsewedy University of Technology–Polytechnic of Egypt, Egypt
Email: mina.youssif@bhit.bu.edu.eg

Abstract - Hydrogen is deemed to be the pivotal substitute for fossil fuels because it has high heating value and zero carbon emissions. Moreover, hydrogen can be produced from renewable sources through alkaline water electrolysis. This study investigates the impact of some operational parameters of alkaline water electrolysis on the gas void fraction. The numerical model of this cell, which consists of the Euler–Euler model and the Secondary current distribution, is solved by the Finite Element method for enhancing the gas void fraction. This research first studies the influence of the inlet flow of electrolyte on the gas void fraction of the alkaline water electrolysis cell. Subsequently, this analysis observes the effect of the concentration of Potassium hydroxide at 70 °C on the gas void fraction. Hence, this study shows that the gas void fraction in an Alkaline Water Electrolysis System has better performance at a low inlet flow rate of electrolyte. Furthermore, the result of this research has shown that the gas void fraction at 70 °C has a proportional relation with the concentration of Potassium hydroxide up to 6 molarity, and exceeding this value, the relation becomes adverse.

Keywords: Renewable energy; Alkaline water electrolysis; Green hydrogen; Numerical simulation; Euler–Euler two-phase; Secondary current distribution; Concentration of electrolyte.

1. Introduction

The production and consumption of fossil fuels are deemed to be the main culprits of the worldwide interconnected problems that threaten all life on Earth [1]. The increasing concentration of atmospheric carbon dioxide (CO_2) due to the combustion of fossil fuels by human activities continues to be a serious environmental crisis [2]. The burning of various conventional fuels results in the emission of approximately 36 billion metric tons of carbon dioxide (CO_2) into the Earth's atmosphere annually, which in turn contributes significantly to climate change and global greenhouse gas emissions [3]. The use of Hydrocarbon fuels produces air pollution that kills around 8.7 million people, which represents twenty percent of all global deaths [1, 4]. The products of fossil fuel use stand as the biggest risk to both present and future children's well-being while worsening worldwide social inequalities and environmental unfairness [5].

Hydrogen is a turning point clean energy source in the pipeline that can revolutionize the world's energy systems [6]. Counter to conventional fuels, when hydrogen burns, it produces water vapor only, which means that the use of hydrogen as an energy resource eliminates toxic pollutants [7]. With a massive energy content of approximately 39.39 kWh/kg, hydrogen has the energy density per unit weight of around three times that of gasoline; thus, it is a perfect candidate for use in vehicles and large energy storage systems [6]. Hydrogen and fuel cells are central to a sustainable energy future because they offer solutions for reduced emissions and increased energy security across various applications [8]. Expanding the production of hydrogen from renewable power sources is critical over the next few decades. This is necessary for decreasing carbon dioxide emissions and achieving independence from fossil fuels [9]. Hydrogen has been widely regarded as a central component of the world's transition to a net-zero economy by 2050 [10].

https://doi.org/10.17683/ijomam/issue22.v1.14

Hydrogen can be produced from renewable energy by the process of water electrolysis [11]. Among the hydrogen production technologies, Alkaline Water Electrolysis (AWE) is singular because it is much cheaper, scalable, and has Long-term stability, especially in comparison to Proton Exchange Membrane (PEM) and Solid Oxide Electrolysis systems [12, 13]. Also, AWE relies on using low-cost and earth-abundant catalysts such as nickel, avoiding the use of limited and costly metals such as platinum and iridium in PEM systems, thereby offering better material availability and cost handling. Alkaline Water Electrolysis possesses several inherent benefits in hydrogen production, including proven technological maturity with decades of industrial experience, robust and stable system design in operation under varied conditions, lower capital investments compared to other electrolysis technologies, ability to handle fluctuating power supply from renewable energy sources, and compatibility with non-precious metal catalysts that reduce the operating costs and it is therefore a viable and economical choice for mass hydrogen production [14].

Alkaline Water Electrolysis produces hydrogen through the electrochemical decomposition of water into hydrogen and oxygen using alkaline electrolytes such as potassium or sodium hydroxide, with the source of electrical energy, despite its technological maturity, AWE is plagued with challenges of energy loss through overpotentials, efficiency loss due to bubble buildup, and ohmic loss due to ionic transport limits, with performance relying on variables such as electrode morphology, composition of electrolyte, temperature, and current density [15].

This AWE cell has a myriad of parameters, which are deemed to be major contributors to increasing hydrogen production. Moreover, recent research papers have been promising, which may optimize AWE at better operating parameters. For instance, it has been indicated that temperature impacts AWE efficiency directly. Improved temperature generally enhances AWE performance, particularly at higher current density. Moreover, thermal homogeneity in stacks of an electrolyzer is observed to enhance efficiency significantly if the right optimized electrolyte flow rate is used. That research paper, Jang et al, findings show that minimizing temperature gradients along the stack is a significant methodology in decreasing energy needs and increasing the economic viability of AWE technology compared to conventional methods in hydrogen production [16]. In addition, A recent paper, Babay et al, studied and compared the investigates the effects of different potassium hydroxide (KOH) concentrations and separator porosities on the gas void fraction [17].

It was found that increasing separator porosities and concentrations are the main contributors to increasing the gas void fraction [17]. On the other hand, A recent study, Xia et al, has further investigated the effect of electrode surface architecture on the efficiency of alkaline water electrolysis using micro-nano surface electrodes compared to traditional flat electrodes. That study utilizes six electrode geometries—rectangular, triangular, trapezoidal, and their inverse shapes—are compared with varied parameters (distance, height, width: 0.5–1 μm) in 3 M KOH at 70°C, suggesting micro-nano electrodes reduce cathode overpotential by up to 65.31% and increase void fraction by 54.53% under the best rectangular designs of the micro-nano electrode [18].

While several previous research studies have inspected alkaline water electrolyzers (AWE) in efficiency for hydrogen production, most of them concentrated on electrochemical performance without fully considering the multiphase nature of gas evolution. Particularly, limited attempts have been made to describe how working conditions, such as electrolyte concentration and flow rate in the inlet, directly influence gas void fraction distribution and how it further influences system performance. Most works that are available simulate simplified electrical performance without observing gas void fraction. Most recent numerical studies of alkaline water electrolyzers (AWE) have restricted the investigation of electrolyte concentration to values below 3 M KOH, mainly to simplify the treatment of transport properties. However, such limitations do not reflect practical operating conditions. Experimental and industrial AWE systems typically employ a higher concentration than 3M to achieve maximum ionic conductivity and reduce ohmic resistance within the cell [19, 20]. This study bridges that gap by developing a more coupled CFD-based Euler–Euler two-phase model with direct correlation between electrolyte concentration and flow rate and gas void fraction, thereby achieving a better understanding of how these parameters influence overall system performance. Respectively. The work was conducted using a numerical model, which will be solved using COMSOL, because the numerical model has high accuracy and low cost. A recent paper has shown that COMSOL has been widely used by various studies in the same application. The reconciliation between the COMSOL and experimental results was found to be excellent, with mean relative absolute difference error (MRADerror) always less than 0.51%, never higher than 1% in all experiments [21]. Hence, the variation of the average gas void fraction with the inlet velocity and concentration will be studied using COMSOL Multiphysics.

2. Model

2.1 Physical Model

An alkaline water electrolyzer operates on the principle of electrochemical water splitting to produce hydrogen and oxygen gases through an alkaline solution [22], generally potassium hydroxide or sodium hydroxide, which is supplied through a bottom inlet. This study selected potassium hydroxide because the performance of KOH is attributed to its higher ionic conductivity and purity, which reduces electrical energy losses due to parasitic reactions observed in NaOH cells under the same conditions [23]. The suitable range of KOH is around 20 to 30 wt.% KOH[4M-7M] based on operation temperature, which is in the range 50°C to 80°C [9]. The cell consists of two electrodes—a positive anode and a negative cathode—separated by a permeable membrane. At the anode, water is oxidized to form oxygen gas and releases electrons, whereas the cathode serves as the location for the reduction of water to form hydrogen gas by gaining electrons. The membrane allows hydroxide ions to pass through, while the gases evolved are separated by it, with oxygen and hydrogen being tapped using top-mounted outlets to reach high gas purity and secure safe and efficient operation of the electrolyzer [13, 24]. Electrode area, electrolyte concentration, and temperature are the key operational parameters that influence voltage requirement, current flow, and system efficiency. In accordance with Faraday's electrochemical laws, the AWE improvement trials aim to reduce the losses of energy through electrical resistance, bubble interference, and electrode activation losses, in accordance with known research practices.

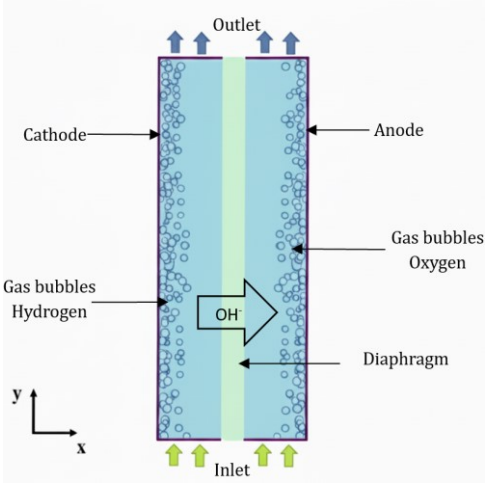

Figure 1: Schematic illustration of the two-dimensional geometric model of the alkaline water electrolyzer

Cathode reaction $2H_2O + 2e^- \rightarrow 2OH^- + H_2$ (1)

Anode reaction $2OH^- \rightarrow 1/2O_2 + H_2O + 2e^-$ (2)

2.2 Mathematical Model

In the current study, the secondary current distribution model was used to obtain the effect of electrode kinetics on the current density distribution, which cannot be considered for the primary distribution. By introducing activation overpotentials through the Butler–Volmer equation, the secondary model provides a more accurate simulation of electrochemical reactions, especially at the high current densities involved in alkaline water electrolysis. In parallel, the Euler–Euler two-phase model was used to describe the interaction of gas bubbles formed at electrodes with the electrolyte. The model accounts for liquid and gas phases as interpenetrating continua, which makes it possible to predict gas void fraction, bubble-induced flow fields, and their effects on mass transport. The integration of the secondary current distribution with the Euler–Euler model provides a full description of the coupled electrochemical–hydrodynamic processes in alkaline water electrolyzers and facilitates better predictions of performance [18, 25].

To make the analysis computationally practical, the following assumptions were employed:

Gases and liquid phases are assumed to be Newtonian, viscous, and incompressible fluids with constant properties and share a common pressure field. The electrolyte is assumed to be evenly distributed, as the ion distribution doesn't have any considerable effect on the concentration of the electrolyte. The flow is considered to be isothermal and therefore, the energy equation and heat exchange are not considered, and surface tension effects are not considered. Bubble break-up and coalescence are not accounted for, and the diameter of the bubble is considered constant at a fixed current density, with bubble–bubble interaction represented by the turbulent dispersion force. Although the Reynolds number is in the laminar flow range, the model turbulence is utilized to match the experimental result and the realistic measured [26, 27]. Finally, due to the inherent complexity of the alkaline electrolysis model, it is solved in two dimensions at steady state. Including all the above assumptions, the governing equations for the phase can be written as follows [18]:

2.2.1 Secondary Current Distribution Model

The overall cell voltage is calculated by summing up the reversible voltage, ohmic losses, and activation overpotentials of the anode and the cathode, represented by the following equation (3) [28]:

$$U_{\text{cell}} = E_{\text{rev}} + \eta_{\text{ohm}} + \eta_{\text{act,a}}(j) + \eta_{\text{act,c}}(j) \quad (3)$$

Here, E_{rev} represents the reversible voltage (V), η_{ohm} denotes the ohmic overpotential, also the voltage drop between the cathode and the anode can be illustrated using Ohm's law(V)[29]. In addition, $\eta_{act,a}$ and $\eta_{act,c}$ are the activation overpotentials (V) at the anode and cathode, respectively. The current density distribution is governed by Ohm's law and the principle of current conservation equations (4,5), described as [16]:

$$\vec{j} = -\sigma\nabla\varphi \tag{4}$$

$$\nabla \cdot \vec{j} = Q \tag{5}$$

Where $\vec{j}$ is the current density vector (A m^{-2}), σ is the electrolyte conductivity (S m^{-1}), φ is the electrical potential (V), and Q is a general current source term (A m^{-3}). The electrode kinetics are modeled using the Butler-Volmer equation (6) to describe the local charge transfer current density [30]:

$$j_{loc} = j_0\left[\exp\left(\frac{\alpha_a F\eta}{RT}\right) - \exp\left(-\frac{\alpha_c F\eta}{RT}\right)\right] \tag{6}$$

In this equation, j_{loc} is the local charge transfer current density (A m^{-2}), j_0 is the exchange current density (A m^{-2}), α_a and α_c are the anodic and cathodic charge transfer coefficients, respectively, η is the activation overpotential (V), F is the Faraday constant (C mol^{-1}), R is the universal gas constant (J mol^{-1} K^{-1}), and T is the temperature (K).

2.2.2 Fluid Dynamics Two-Phase Model

The two-phase flow in the AWE is simulated using the Euler-Euler model [31], which is suitable for capturing the macroscopic behavior of gas and liquid phases. This model calculates the void fraction of each phase without tracking individual bubbles, assuming both phases share a common pressure field. The dynamics of each phase are governed by the continuity equations and momentum (8,9):

$$\alpha_g + \alpha_l = 1 \tag{7}$$

$$\frac{\partial}{\partial t}\left(\alpha_g\rho_g + \alpha_l\rho_l\right) + \nabla \cdot \left(\alpha_g\rho_g\overrightarrow{u_g} + \alpha_l\rho_l\overrightarrow{u_l}\right) = 0 \tag{8}$$

$$\frac{\partial}{\partial t}(\rho_k\,\alpha_k\,\vec{u}_k) + \nabla(\rho_k\,\alpha_k\vec{u}_k\vec{u}_k) = \alpha_k\,\rho_k\,\vec{g} - \alpha_k\nabla p + \nabla\cdot(\alpha_k\tau_k) + \vec{F}_k \tag{9}$$

Here, $\vec{u}$ is the velocity (m s^{-1}), p is the pressure (Pa), α is the void fraction, ρ is the density (kg m^{-3}), $\vec{g}$ is the gravitational acceleration (m s^{-2}), τ is the stress tensor (N m^{-2}), and $\vec{F}$ k is the volume force (N m^{-3}), with subscript k denoting the gas (g) or liquid (l) phase. To account for turbulence, the k-ε model is employed, solving turbulent kinetic energy k (m^2 s^{-2}) and dissipation rate ε (m^2 s^{-3}):

$$\tau_k = (\mu_k + \mu_T)\left(\nabla\vec{u}_k + (\nabla\vec{u}_k)^T - \frac{2}{3}(\nabla\cdot\vec{u}_k)I\right) - \frac{2}{3}\rho_k kI \tag{10}$$

$$\mu_T = \rho_k C_\mu\frac{k}{\epsilon} \tag{11}$$

$$\rho\frac{\partial k}{\partial t} + \rho\vec{u}\cdot\nabla k = \nabla\cdot\left(\left(\mu + \frac{\mu_T}{\sigma_k}\right)\nabla k\right) + P_k - \rho\epsilon \tag{12}$$

$$\rho\frac{\partial \epsilon}{\partial t} + \rho\vec{u}\cdot\nabla\epsilon = \nabla\cdot\left(\left(\mu + \frac{\mu_T}{\sigma_\epsilon}\right)\nabla\epsilon\right) + C_{\epsilon,1}\frac{\epsilon}{k}P_k - C_{\epsilon,2}\rho\frac{\epsilon^2}{k} \tag{13}$$

Where μ is the viscosity (Pa s), μT is the turbulent viscosity (Pa s), I is the unit tensor, C_μ, $C_{\varepsilon,1}$, $c_{\varepsilon,2}$, and σ_k are turbulence model constants, and P_k accounts for bubble-induced turbulence. Drag and turbulent dispersion forces are included to model bubble interaction equations(14,15) [32]:

$$\vec{F}_D = -\frac{3}{4}\rho_k\alpha_k\frac{C_d}{d_b}|\vec{U}_r|\vec{U}_r \tag{14}$$

$$\vec{F}_{BD} = -\rho_k\alpha_k\frac{k_g}{d_b}|\vec{U}_r|\nabla\alpha_k \tag{15}$$

Where C_d is the drag coefficient, Kg is the diffusion factor, d_b is the bubble diameter, and $\vec{U}_r$ is the relative velocity. The drag coefficient follows the Schiller-Naumann model [33]

$$C_d = \frac{24}{Re}(1 + 0.15Re^{.687}) \text{ at Re<1000}$$
$$C_d = 0.44 \quad \text{at Re >1000} \tag{16}$$

Where R_e is the Reynolds number:

$$\mathrm{Re} = \frac{\rho_l|\overrightarrow{U_r}|d_b}{\mu_l} \tag{17}$$

The gas void fraction transport is described by:

$$\frac{\partial(\alpha_g\rho_g)}{\partial t} + \nabla\cdot\left(\alpha_g\rho_g\overrightarrow{u_g}\right) = -\dot{m_{gl}} \tag{18}$$

Where $\dot{m_{gl}}$ Is the mass transfer rate from gas to liquid (kg m^{-3} s^{-1}). The gas generation rate at the electrode surface (kg m^{-2} s^{-1}) is determined using the Faraday equation (19):

$$\dot{m_g} = \frac{j\cdot M_g}{nF} \tag{19}$$

Where M_g is the molar mass of the gas (kg mol^{-1}), and n is the number of transferred electrons.

Electrochemical performance degradation in alkaline electrolyte systems arises principally from bubble-induced effects, manifesting as both (i) decreased ionic conductivity due to bubble obstruction of charge transport pathways, and (ii) reduced catalytic activity from bubble coverage of electrode active sites. Following established methodologies, these coupled effects are mathematically represented through the Bruggeman correction, with an equation describing the modified electrolyte conductivity and an equation characterizing the effective exchange current density that accounts for surface coverage effects [30]:

$$i_{\text{eff}} = i_0(1-\alpha_g)^{1.5} \tag{20}$$

$$\sigma_{\text{eff}} = \sigma_0(1-\alpha_g)^{1.5} \quad (21)$$

2.3 Implementation of Boundary Conditions in Numerical Simulations:

The interfacial conditions governing the Multiphysics coupling are systematically implemented as shown in Figures 1 and 2. The electrochemical domain boundaries are treated as electrically insulating surfaces, while the hydrodynamic solution domain employs conventional flow boundary conditions (velocity inlet, pressure outlet) combined with no-slip wall conditions at all solid boundaries (u = 0 m s^{-1}). Of particular significance is the implementation of: (i) reactive mass transport boundary conditions at electrode surfaces to capture gas evolution effects, and (ii) the direct mapping of OH^- flux from the electrochemical solution to establish the liquid phase mass flux boundary condition at the porous diaphragm interface, also for the electrolysis of water.

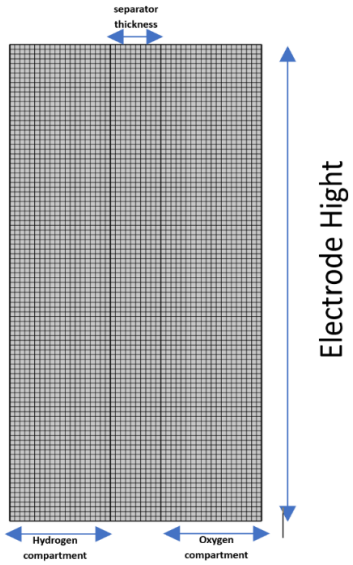

Figure 2. Grid layout of the AWE cell

To solve this numerical model, take the operation parameter and boundary condition from Table 1.

Table 1. Operation parameters and boundary

Symbol	Value	Unit	Description
R	8.314	J mol^{-1} K^{-1}	Universal gas constant
F	96,485.3	C mol^{-1}	Faraday constant
W_{H_2}	2	mm	Hydrogen compartment depth
W_{sep}	1	mm	Separator thickness
W_{O_2}	2	mm	Oxygen compartment depth
H_{elec}	1	cm	Electrode length
d_{bubble}	200	µm	Bubble size
T	70	°C	Working temperature
P	1	atm	Pressure
i_{0H_2}	100	A m^{-2}	Exchange current, hydrogen oxidation
i_{0O_2}	1	A m^{-2}	Exchange current, oxygen reduction
M_{H_2O}	18	g mol^{-1}	Water molecular weight
M_{H_2}	2	g mol^{-1}	Hydrogen molecular weight
M_{O_2}	32	g mol^{-1}	Oxygen molecular weight
M_{OH}	17	g mol^{-1}	Hydroxide molecular weight
C_{KOH}	1 to 7	M	Electrolyte solution strength
v_{in}	0.05 to 0.3	m s^{-1}	Mean inlet speed

3. Cross-validation with Earlier Studies

In this study, the validation of the numerical model is achieved by comparing the results with the recent paper's results, which were obtained under the same operating conditions [18]. According to a recent paper, the average gas void fraction at the surface of the flat electrode is 2.15% at conditions (70 °C and the diameter of bubbles is 200µm) when using a triangular mesh with the mesh elements that were fine predefined on the electrolyte domain and extra fine on the electrodes and diaphragm boundaries. This study used quadrilateral meshes with mesh elements that were extremely fine, predefined on the all domain of the cell and boundaries. In this study, the extremely fine predefined mesh in COMSOL Multiphysics was used to provide the highest available refinement, ensuring accurate resolution of near-wall flow and gas–liquid interface gradients without requiring a boundary-layer mesh. Unlike the reference study that employed a fine mesh with additional boundary-layer refinement, the present

model achieved higher element density across the domain, making further layering unnecessary. Also, this paper achieved approximately the same value, which is 2.0854%. The difference in the recent paper value and this study's value is 3% due to in this study increasing number of elements. Figure 3 shows the gas distribution in the recent study compared to this study.

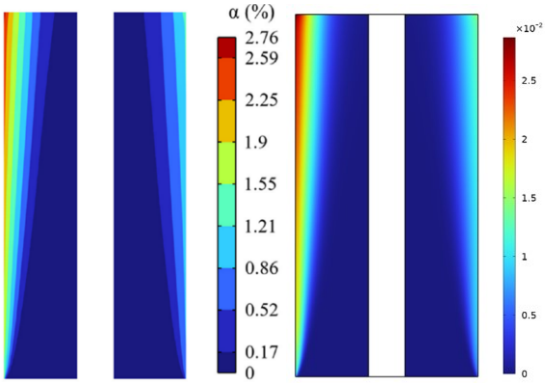

a *b*

Figure 3. The gas void fraction distribution (a) the study Xia, Y. et al. (Materials) (b) this study.

4. Numerical Results

The impact of the electrolyte concentration and inlet electrolyte velocity on the gas void fraction at 70 °C has been studied numerically. The numerical model was solved using the Finite Element method, and the mesh decomposition was conducted.

4.1 Effect of the Inlet Velocity of Gas Void Fraction

The simulations were conducted at a constant operating temperature of 70 °C and a set cell voltage of 2 V. The inlet feed velocity varies from 0.05 m/s to 0.3 m/s with a 0.05 m/s step to study their influence on the gas volume fraction distribution throughout the electrolyzer domain, as shown in Figure 4 for maximum and minimum inlet velocity.

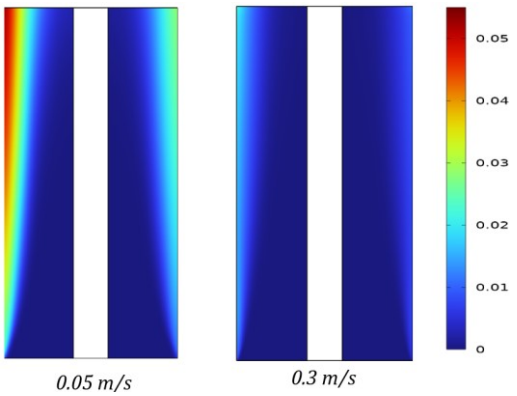

Figure 4: The gas void fraction distribution electrode for maximum and minimum inlet velocity (U = 2V)

After analyzing Figure 4, it can be noticed that the huge number of bubbles that lead to the maximum void fraction is at the surface of the cathode and the top of the gas compartment. Also, two lines were selected in this study as primary observation lines: the top of the compartment and the surface of the electrode. The top of the compartment is where bubbles, having been formed, travel upward and accumulate before leaving the electrolyzer. The behavior of the gas phase in this area directly affects the efficiency with which hydrogen can be removed from the system. Bubble over-accumulation near the outlet increases electrical resistance and hinders mass transfer, hence decreasing the overall efficiency of the electrolyzer.

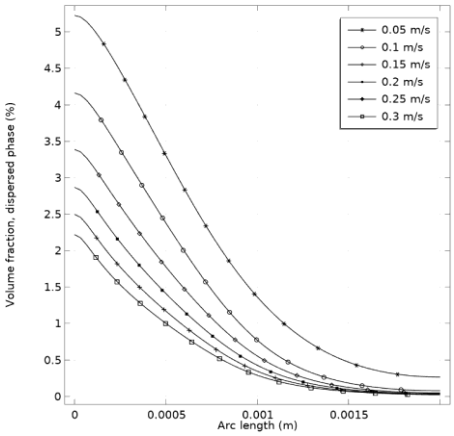

Figure 5: Gas void fraction profiles at the top of the hydrogen compartment under different inlet velocities (U = 2 V)

The electrode surface, on the other hand, is the initial site where bubbles are created. Adherent gas bubbles covering or adhering to the electrode can jam active catalytic sites, which deteriorates the electrochemical reaction and increases the overpotential. Therefore, the investigation of void fraction distribution over the electrode surface is vital in the examination of the effect of electrode design on bubble release.

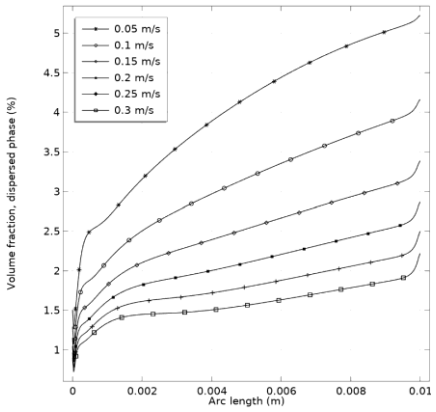

Figure 6: Gas void fraction profiles for the surface of the cathode under different inlet velocities (U = 2 V)

Table 2. The average void fraction of the surface electrode under varying inlet velocities(U=2V)

Inlet velocity	Average Void Fraction (%)
0.05	4.0028
0.1	3.0771
0.15	2.4841
0.2	2.0854
0.25	1.7978
0.3	1.5805

The gas void fraction on the electrode surface for the hydrogen gas compartment at different inlet velocities is illustrated in Figure 6. Then the average value of the gas void fraction for every line in Figure 6 is taken and put in Table 2. According to these results, the gas void fraction decreases when increasing the inlet velocity for electrolyte in the AWE cell because increasing inlet velocity removes bubbles that leads to reduce the gas void fraction that is shown in Figure 6; Moreover, Table 2 accentuates that the mean void fraction of the gas on the surface of the electrode increased from 1.5805% to 4.0028% when decreasing the inlet velocity from 0.3 m/s to 0.05 m/s.

4.2 The Effect of the Concentration of Electrolyte

This study illustrates the impact of the concentration of electrolyte on the average void fraction, a recent research paper that studies the impact of the concentration of solution when the assumed model is laminar, and up to 3M [17]. In this study, it is solved as a turbulent model [26, 27]. Additionally, this study increases the range of concentrations. Figure 7 describes the distribution of gas void fraction of the AWE cell under different concentrations.

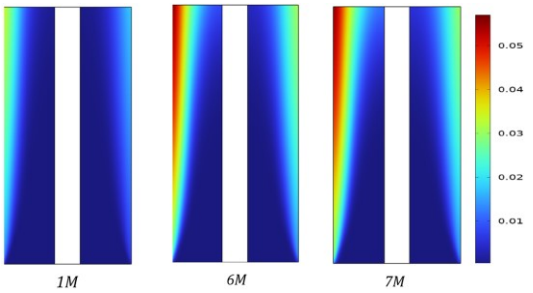

Figure 7: The gas void fraction distribution of the electrode for different concentrations of electrolyte (U = 2V).

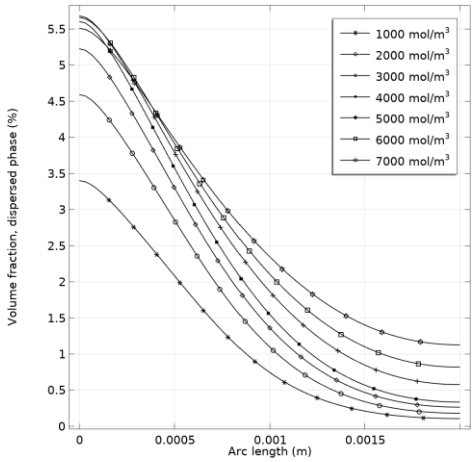

Figure 8: Variation of gas void fraction at the top of the hydrogen compartment under different electrolytes (U=2V)

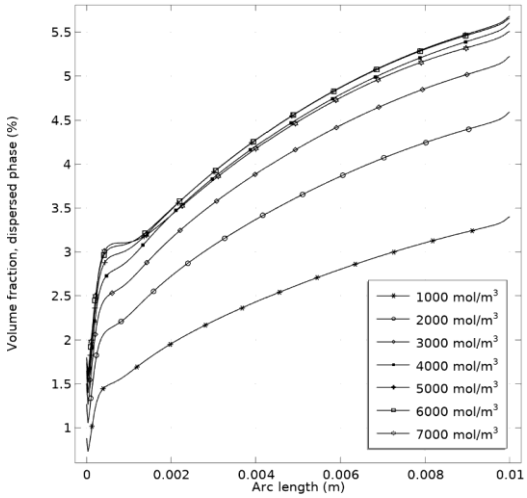

Figure 9: Cathode surface gas void fraction profiles under varying electrolyte concentrations (U=2V)

Table 3. The average void fraction of the surface electrode under varying KOH concentrations (U=2V)

Concentration[M]	Average Void Fraction (%)
1	2.5221
2	3.4765
3	4.0028
4	4.3228
5	4.4080
6	4.4146
7	4.3221

The gas void fraction for the surface of the cathode for different concentrations of KOH is shown in Figure 9. This study also calculates the average of the gas void fraction for every concentration from Figure 9 and puts it in Table 3. According to figures 7,8,9, and table 3, the average gas void fraction at the surface of the cathode soars from 2.5221% at 1M concentration to 4.4146% at 6M, then diminishes to 4.3221% at 7M. This means that the suitable concentration of KOH is 6M at 70°C. According to recent studies, the ionic conductivity of KOH increases with concentration to an optimum value, typically in the range 5–8M, depending on temperature, beyond which it declines with enhanced ion–ion interaction and viscous effects. This is observed at all temperatures, although rising temperatures enhance the optimum conductivity and widen the concentration range of KOH somewhat, with maximum values of 6–7M sometimes reported at 70°C [34-36]. Hence, what can be observed from these results is that the gas void fraction increases when the KOH concentration increases from 1M to 6M, but when the concentration is increased to 7M, the gas void fraction starts to plummet because of the reduction in conductivity and increasing viscosity. This means that the optimum concentration of KOH at 70°C doesn't exceed 6M.

5. Conclusions

This study has employed computational analysis to investigate the relationship between the average void fraction at the surface of the electrode and the inlet velocity and concentration of electrolyte.

According to this study, Table 3 and Figure 4 illustrate the impact of varying inlet velocity on the gas void fraction distribution. What can be said is that the average void fraction has an inverse relationship with the inlet velocity of the electrolyte.

Furthermore, the findings demonstrate the effect of the concentration of KOH at 70°C. It was found that the gas void fraction grows when the KOH concentration rises until the concentration reaches a critical value, which is 6M. Then the gas void fraction starts to plummet when the concentration exceeds 6M.

In conclusion, after this study has manifested the points mentioned above, it revealed that enhancing the gas void fraction depends on reducing the inlet velocity of electrolyte, as well as increasing the concentration of KOH until 6M at 70°C.

References

[1] S. Wolf *et al.*, "Scientists' warning on fossil fuels," *Oxford Open Climate Change,* vol. 5, no. 1, p. kgaf011, 2025.

[2] S. C. Doney, V. J. Fabry, R. A. Feely, and J. A. Kleypas, "Ocean acidification: the other CO2 problem," *Annual review of marine science,* vol. 1, no. 1, pp. 169-192, 2009.

[3] K. Uddin, "Nuclear energy, environment and public safety: north-south politics," *Strategic Planning for Energy and the Environment,* vol. 38, no. 4, pp. 31-41, 2019.

[4] K. Vohra, A. Vodonos, J. Schwartz, E. A. Marais, M. P. Sulprizio, and L. J. Mickley, "Global mortality from outdoor fine particle pollution generated by fossil fuel combustion: Results from GEOS-Chem," *Environmental research,* vol. 195, p. 110754, 2021.

[5] F. Perera, "Pollution from fossil-fuel combustion is the leading environmental threat to global pediatric health and equity: Solutions exist, "*International journal of environmental research and public health,* vol. 15, no. 1, p. 16, 2018.

[6] Y. Manoharan *et al.*, "Hydrogen fuel cell vehicles; current status and future prospect," *Applied Sciences,* vol. 9, no. 11, p. 2296, 2019.

[7] D. Le Bideau *et al.*, "Evolutionary design optimization of an alkaline water electrolysis cell for hydrogen production," *Applied Sciences,* vol. 10, no. 23, p. 8425, 2020.

[8] P. P. Edwards, V. L. Kuznetsov, W. I. David, and N. P. Brandon, "Hydrogen and fuel cells: Towards a sustainable energy future," *Energy policy,* vol. 36, no. 12, pp. 4356-4362, 2008.

[9] J. Brauns and T. Turek, "Alkaline water electrolysis powered by renewable energy: A review," *Processes,* vol. 8, no. 2, p. 248, 2020.

[10] S. G. Nnabuife *et al.*, "The prospects of hydrogen in achieving net zero emissions by 2050: A critical review," *Sustainable Chemistry for Climate Action,* vol. 2, p. 100024, 2023.

[11] D. M. Santos, C. A. Sequeira, and J. L. Figueiredo, "Hydrogen production by alkaline water electrolysis," *Química Nova,* vol. 36, pp. 1176-1193, 2013.

[12] J. C. Ehlers, A. A. Feidenhans'l, K. T. Therkildsen, and G. O. Larrazábal, "Affordable green hydrogen from alkaline water electrolysis: key research needs from an industrial perspective," *ACS Energy Letters,* vol. 8, no. 3, pp. 1502-1509, 2023.

[13] S. S. Kumar and H. Lim, "An overview of water electrolysis technologies for green hydrogen production," *Energy reports,* vol. 8, pp. 13793-13813, 2022.

[14] A. L. Santos, M.-J. Cebola, and D. M. Santos, "Towards the hydrogen economy—A review of the parameters that influence the efficiency of alkaline water electrolyzers," *Energies,* vol. 14, no. 11, p. 3193, 2021.

[15] S. Dash, A. Singh, S. K. Surapraraju, and S. K. Natarajan, "Advances in green hydrogen production through alkaline water electrolysis: A

comprehensive review," *International Journal of Hydrogen Energy,* vol. 83, pp. 614-629, 2024.

[16] D. Jang, W. Choi, H.-S. Cho, W. C. Cho, C. H. Kim, and S. Kang, "Numerical modeling and analysis of the temperature effect on the performance of an alkaline water electrolysis system," *Journal of Power Sources,* vol. 506, p. 230106, 2021.

[17] M.-A. Babay, M. Adar, A. Chebak, and M. Mabrouki, "Dynamics of gas generation in porous electrode alkaline electrolysis cells: An investigation and optimization using machine learning," *Energies,* vol. 16, no. 14, p. 5365, 2023.

[18] Y. Xia, M. Gao, J. Yu, Y. Si, L. Chen, and S. Mei, "Numerical Study on Hydrodynamic Characteristics and Electrochemical Performance of Alkaline Water Electrolyzer by Micro-Nano Surface Electrode," *Materials,* vol. 15, no. 14, p. 4927, 2022.

[19] H. Tüysüz, "Alkaline water electrolysis for green hydrogen production," *Accounts of Chemical Research,* vol. 57, no. 4, pp. 558-567, 2024.

[20] N. Thissen *et al.*, "Industrially Relevant Conditions in Lab-Scale Analysis for Alkaline Water Electrolysis," *ChemElectroChem,* vol. 11, no. 1, p. e202300432, 2024.

[21] J. Rodríguez and E. Amores, "CFD modeling and experimental validation of an alkaline water electrolysis cell for hydrogen production," *Processes,* vol. 8, no. 12, p. 1634, 2020.

[22] C. Hu, L. Zhang, and J. Gong, "Recent progress made in the mechanism comprehension and design of electrocatalysts for alkaline water splitting," *Energy & Environmental Science,* vol. 12, no. 9, pp. 2620-2645, 2019.

[23] M. H. Sellami and K. Loudiyi, "Electrolytes behavior during hydrogen production by solar energy," *Renewable and Sustainable Energy Reviews,* vol. 70, pp. 1331-1335, 2017.

[24] P. Vermeiren, J. Moreels, A. Claes, and H. Beckers, "Electrode diaphragm electrode assembly for alkaline water electrolysers," *International Journal of Hydrogen Energy,* vol. 34, no. 23, pp. 9305-9315, 2009.

[25] F. F. Rivera, T. Pérez, L. F. Castañeda, and J. L. Nava, "Mathematical modeling and simulation of electrochemical reactors: A critical review," *Chemical engineering science,* vol. 239, p. 116622, 2021.

[26] K. Aldas, N. Pehlivanoglu, and M. D. Mat, "Numerical and experimental investigation of two-phase flow in an electrochemical cell," *international journal of hydrogen energy,* vol. 33, no. 14, pp. 3668-3675, 2008.

[27] P. Boissonneau and P. Byrne, "An experimental investigation of bubble-induced free convection in a small electrochemical cell," *Journal of Applied Electrochemistry,* vol. 30, no. 7, pp. 767-775, 2000.

[28] A. S. Tijani, N. A. B. Yusup, and A. A. Rahim, "Mathematical modelling and simulation analysis of advanced alkaline electrolyzer system for hydrogen production," *Procedia Technology,* vol. 15, pp. 798-806, 2014.

[29] R. Phillips, A. Edwards, B. Rome, D. R. Jones, and C. W. Dunnill, "Minimising the ohmic resistance of an alkaline electrolysis cell through effective cell design," *International Journal of Hydrogen Energy,* vol. 42, no. 38, pp. 23986-23994, 2017.

[30] J. Newman and N. P. Balsara, *Electrochemical systems*. John Wiley & Sons, 2021.

[31] M. Ishii and T. Hibiki, *Thermo-fluid dynamics of two-phase flow*. Springer Science & Business Media, 2010.

[32] A. Troshko and Y. Hassan, "A two-equation turbulence model of turbulent bubbly flows," *International Journal of Multiphase Flow,* vol. 27, no. 11, pp. 1965-2000, 2001.

[33] L. Schiller, "A drag coefficient correlation," *Zeit. Ver. Deutsch. Ing.,* vol. 77, pp. 318-320, 1933.

[34] R. A. Marquez *et al.*, "A guide to electrocatalyst stability using lab-scale alkaline water electrolyzers," *ACS Energy Letters,* vol. 9, no. 2, pp. 547-555, 2024.

[35] M. Schalenbach, A. R. Zeradjanin, O. Kasian, S. Cherevko, and K. J. Mayrhofer, "A perspective on low-temperature water electrolysis–challenges in alkaline and acidic technology," *International Journal of Electrochemical Science,* vol. 13, no. 2, pp. 1173-1226, 2018.

[36] R. J. Gilliam, J. Graydon, D. Kirk, and S. Thorpe, "A review of specific conductivities of potassium hydroxide solutions for various concentrations and temperatures," *International Journal of Hydrogen Energy,* vol. 32, no. 3, pp. 359-364, 2007.